NON-NEWTONIAN OSCILLATORY BOUNDARY LAYER, A NUMERICAL APPROACH

Ondřej WEIN and Václav SOBOLÍK

Institute of Chemical Process Fundamentals, Czechoslovak Academy of Sciences, 165 02 Prague 6 — Suchdol

Received December 17th, 1984

Differential schemes have been constructed by using the integro-differential formulation of the equations of motion in stresses. The problem of periodic flow of the purely-viscous non-Newtonian liquid on a harmonically oscillating plate has been solved numerically for extremally high values of the Reynolds number. The velocity and stress fields as well as estimates of the flow enhancement E are given for the quasi-oscillatory regime, Fr $\to \infty$, for the pseudoplastic liquid with the extremally low flow index, $n = 0{\cdot}15$.

The flow of a layer of the power-law liquid, generated by an oscillating flat plate, can be taken as a model problem in the theory of vibrational flow enhancement[1,2]. The formulation of the problem consists of the equation of motion for the normalized fields of longitudinal velocity $V(Y, T)$ and shear stress $S(Y, T)$:

$$\partial_T V = -\partial_Y S\,, \tag{1}$$

the constitutive equation of the inelastic power-law liquid,

$$\partial_Y V = [-S]^m = -[S]^m\,, \tag{2}$$

the kinematic boundary condition on oscillating plate

$$V = V_0(T) \quad \text{for} \quad Y = 0\,, \tag{3}$$

the dynamic boundary condition on free surface

$$S = 0 \quad \text{for} \quad Y = H\,, \tag{4}$$

and the antiperiodicity conditions in the while volume of the liquid

$$V|_{T+\pi} = -V|_T\,, \quad S|_{T+\pi} = -S|_T\,. \tag{5a, b}$$

This formulation of the boundary-value problem can be transformed to the parabolic problem in velocities[1]

$$\partial_T V = \partial_Y [\partial_Y V]^n , \tag{6}$$

$$V|_{Y=0} = V_0(T) , \quad \partial_Y V|_{Y=H} = 0 , \tag{7), (8}$$

or in stresses[2]

$$\partial_T [S]^m = \partial_{YY}^2 S , \tag{9}$$

$$\partial_Y S|_{Y=0} = A(T) , \quad S|_{Y=H} = 0 , \tag{10), (11}$$

where both $V_0(T)$ and $A(T)$,

$$A(T) = -\mathrm{d}_T V_0(T) \tag{12}$$

are antiperiodic functions normalized by the condition

$$\max |A(T)| = 1 . \tag{13}$$

A simple asymptotic solution, the so-called *creeping asymptote*[3], can be found for $H \ll 1$:

$$S = A(T)(H - Y) , \tag{14}$$

$$V = V_0(T) - [A(T)]^m \frac{H^{m+1} - (H - Y)^{m+1}}{m + 1} , \tag{15}$$

with any functions $V_0(T)$ or $A(T)$.

A corresponding asymptotic solution for $H \gg 1$, the so-called *boundary-layer asymptote*, is known only for the harmonic oscillations of constitutively linear liquids, *e.g.* for the Newtonian liquid,

$$V_0(T) = \cos T , \quad A(T) = \sin T , \tag{16a, b}$$

$$S = \sin (T - Y/\sqrt{2} - \pi/4) \exp (-Y/\sqrt{2}) , \tag{17}$$

$$V = \cos (T - Y/\sqrt{2}) \exp (-Y/\sqrt{2}) . \tag{18}$$

Analytical approximate approaches to the corresponding non-linear problems have not been succesfull even for purely-viscous pseudoplastic liquids[4,5]. Thus, a numerical treatment of the problem seems to be the only convenient way.

In the theory of vibrational flow enhancement[2], the problem of purely oscillatory boundary-layer flow, $1 \ll H$, without a net steady component has straightforward application in the asymptotic estimate of the flow enhancement under quasi-oscillatory conditions, $1 \ll \mathrm{Fr}$. The ratio E of the mean flow rates on the oscillating and fixed plate for the same film thicknesses is given by[2]

$$E \approx 1 + \varkappa(m, \infty)\, H^{-m}\, \mathrm{Fr}^{m-1}\,, \tag{19}$$

where

$$\varkappa(m, H) = m(m+2) \int_0^H \langle |S|^{m-1} \rangle (1 - Y/H)^2 \,\mathrm{d}Y\,. \tag{20}$$

The problem can also serve as a model example for testing both the approximate analytic approaches and the computer programs developed for attacking other parabolic boundary-value problems in the theory of oscillatory flows of constitutively non-linear liquids. This last point has recently been gaining ground because many computer programs working well in the linear case, $m = 1$, or in the low-H regime, tend to lose the accuracy seriously or to break down totally in the non-linear and high-H cases[6].

Difference schemes[7] are presented and tested here which converge to an anti-periodic solution even for the extremally difficult cases $m \gg 1$, $H \gg 1$.

Discrete Representations, Error Parameters

The velocity and stress fields are represented by two-dimensional matrices of the corresponding values

$$V_j^i = V(Y_j, T^i)\,, \quad S_j^i = S(Y_j, T^i) \tag{21a, b}$$

in the mesh points (Y_j, T^i)

$$T^i = T_0 + (i-1)\,\mathrm{D}T, \quad i = 1, \ldots, 2M+1 \tag{22a}$$

$$Y_j = (j-1)\,\mathrm{D}Y, \quad j = 1, \ldots, N \tag{22b}$$

with the constant but unequal steps on the space and time coordinates

$$\mathrm{D}Y = L/N\,, \quad \mathrm{D}T = \pi/M\,, \tag{23a, b}$$

see also Fig. 1. The mesh points are also considered on all edges of the rectangular domain, *i.e.* for $Y_1 = 0$, $Y_{N+1} = L \leqq H$, $T^1 = T_0$, $T^{2M+1} = T_0 + 2\pi$.

Parabolic nature of the problem enables to construct the periodic solution iteratively, by searching for the initial profiles (B_j^1) of velocities $(B = V)$ or stresses $(B = S)$

which fulfil the periodicity conditions, $(B_j^1) = (B_j^{2M+1})$. The following norms,

$$\varepsilon_P(B) = \|B_j^{2M+1} - B_j^1\|, \quad 1 \leqq j \leqq N, \tag{24a}$$

or

$$\varepsilon_A(B) = \|B_j^{2M+1} + B_j^{M+1}\|, \quad 1 \leqq j \leqq N, \tag{24b}$$

can be introduced as quantitative measure of deviations from the periodicity or antiperiodicity conditions, resp.

However, the error criteria based only on the initial and final profiles can considerably depend on the choice of the initial moment T_0. More realistic error criterion should therefore respect the deviations from the expected time symmetry over the whole domain of the field B, $Y \in \langle 0; H \rangle$, $T \in \langle T_0; T_0 + 2\pi \rangle$. In particular, the norm

$$\varepsilon_A^*(B) = \|B_j^{i+1} + B_j^{i+1+M}\|, \quad 1 \leqq j \leqq N, \quad 0 \leqq i \leqq M, \tag{24c}$$

seems to be an adequate error criterion for testing quantitatively the deviation from the antiperiodicity condition, Eqs (*5a, b*).

It is also necessary to estimate the departure from the unknown exact solution. Besides the cumbersome method of halving the grid spacings, the methods of weighted residuals are widely used. Two types of the weighted residuals are in close relation to the rheodynamic problem under consideration – the relative defect of the instantaneous momentum balance,

$$\varepsilon_M(T) = |S(0, T) - W(T)|/\max |S(0, T)|, \tag{25}$$

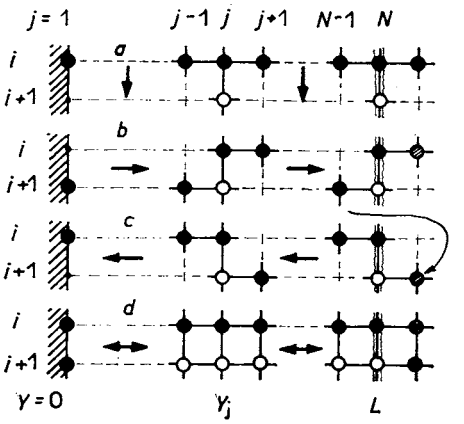

FIG. 1

Finite difference schemes. *a* Explicite scheme, *b* semiimplicite scheme starting at the wall, *c* semiimplicite scheme starting at the surface, *d* implicite scheme. Full points – values known from the initial conditions or previous computations; hatched points – values known from the mirror symmetry about the surface, $j = N$; empty points – computed values

and the relative defect of the total energy balance,

$$\varepsilon_E = |\psi_{work}/\psi_{diss} - 1| . \tag{26}$$

For the exact solution, the quantities $\varepsilon_M(T)$, ε_E should be zero as the non-zero quantities,

$$S(0, T) = [-\partial_Y V|_{Y=0}]^n , \tag{27}$$

$$W(T) = \int_0^H \partial_T V(T, Y)\, dY , \tag{28}$$

$$\psi_{work} = -\langle V_0(T)\, S(0, T)\rangle , \tag{29}$$

$$\psi_{diss} = \int_0^H \langle |S(Y, T)|^{m+1}\rangle\, dY , \tag{30}$$

represent the instantaneous wall stress, the instantaneous inertia force, the total work done by the oscillating plate, and the total dissipated mechanical energy, respectively.

Finite-Difference Representation in Velocities

The constitutive non-linearity of the pseudoplastic type, $n < 1$ or $m > 1$, introduces essential difficulties into the solution of the problem represented by the finite-difference equations in velocities. The well-known explicite difference scheme is considered here as an illustrative example:

$$V_j^{i+1} = V_j^i + \alpha([V_{j+1}^i - V_j^i]^n - [V_j^i - V_{j-1}^i]^n) , \quad 2 \leqq j \leqq N - 1 . \tag{31}$$

In these equations, the velocity values in the inner mesh points, V_j^{i+1}, are the only unknown parameters. All values (V_j^i), $j = 1, \ldots, N$, are known from the trial initial conditions and previous calculations. The value V_1^{i+1} is given by the boundary condition at the harmonically oscillating plate,

$$V_1^{i+1} = \cos(T^{i+1}) . \tag{32}$$

By taking into consideration the mirror symmetry at the free surface, $V_{N+1}^i = V_{N-1}^i$, the Eq. (31) for $j = N$ can be simplified to the form

$$V_N^{i+1} = V_N^i - 2\alpha[V_N^i - V_{N-1}^i]^n . \tag{33}$$

This explicite scheme leads to the discrete approximation of the velocity field with

a satisfactory accuracy only for the linear problem, $n = 1$, if the well-known stability condition[8], $\alpha < 1/2$, is kept. On the other hand, the explicite scheme fails even in weakly non-linear cases, $n \leqq 0{\cdot}8$, at moderate Reynolds numbers, $H \geqq 2$.

The origin of this failure becomes more obvious by considering the equation of motion in the alternate form

$$\partial_T V = n|\partial_Y V|^{-(1-n)} \partial^2_{YY} V. \tag{34}$$

The corresponding quasi-linear explicite scheme,

$$V_j^{i+1} = V_j^i + \alpha^*_{ij}(V^i_{j+1} - 2V_j^i + V^i_{j-1}), \tag{35}$$

contains the parameter α^*_{ij},

$$\alpha^*_{ij} = \frac{n}{2}\alpha(|V^i_{j+1} - V^i_j|^{-(1-n)} + |V^i_j - V^i_{j+1}|^{-(1-n)}), \tag{36}$$

which becomes infinite in the points (Y, T) for which $\partial_Y V = 0$. The existence of such singular points and of the corresponding singular lines $Y = Y^*_{sg}(T)$ follows from both the boundary conditions at $Y = H$ and the antiperiodicity conditions with the half-period $\Delta T = \pi$. In particular, there exists subdomain $Y \subset (Y_H, H)$ within which the scheme (35) is globally unstable due to the inequality $\alpha^*_{i,j} > 1/2$.

The global instability can be suppressed by using the semiimplicite schemes[7], see also Fig. 1*b*. Only immaterial local instabilities appear in the region $Y \in (Y_H, H)$ manifesting themselves by slight oscillations of the velocity values about the corresponding smoothed courses. Nevertheless, the existence of singular lines indicates a possible appearance of considerable discretization errors for any finite-difference representation of the problem in velocities, at least in a close neighbourhood of the singular lines.

The accuracy of discrete approximation based on the semi-implicite scheme was tested by using Kutta's method of halving the grid spacings as well as by computing the weighted residuals ε_M, ε_E. The differences between values (V_j^i) in the common mesh points of the grids with $(N, M) = (10, 50)$ and $(N, M) = (20, 100)$ were found to be negligible in all tested cases, $n \geqq 0{\cdot}5$. On the other hand, the momentum defect ε_M attained values about $0{\cdot}1 \div 0{\cdot}5$ in the neighbourhood of the singular points, $\partial_Y V|_{Y=0} = 0$, and the energy defect ε_E was not less than 0·05. It can be concluded from these results that the weighted residuals provide more strict (and time saving) test of the accuracy than Kutta's method.

Similar results have been obtained by using the implicite schemes of Crank–Nicolson type. A question of actual accuracy of the velocity fields determined by solving the problem in velocities has been answered only by considering the same problem in stresses.

FINITE-DIFFERENCE REPRESENTATION IN STRESSES

Preliminary numerical experiments have shown that neither explicite schemes in stresses,

$$[S_j^{i+1}]^m = [S_j^i]^m + 2\beta(S_{j+1}^i - 2S_j^i + S_{j-1}^i), \tag{37}$$

with

$$2\beta = DT/DY^2, \tag{38}$$

nor corresponding semiimplicite schemes warrant results with higher accuracy than current methods of solving the problem in velocities. On the contrary, these schemes have shown certain instabilities even in the cases $H \ll 1$, *i.e.* in regimes for which the semiimplicite schemes in velocities were stable. The cause of these instabilities is apparent from the following alternate expression of the explicite scheme,

$$S_j^{i+1} = S_j^i + \beta_{ij}^*(S_{j+1}^i - 2S_j^i + S_{j-1}^i), \tag{39}$$

$$\beta_{ij}^* = \beta/(m|S_j^i|^{m-1}), \tag{40}$$

which is a finite-difference representation of the equation of motion in the form $\partial_T S = \partial_{YY}^2 S/(m|S|^{m-1})$. It holds $S \to 0$ and $\beta_{ij}^* \to \infty$ for $Y \to H$. The transition from the quasi-linear scheme (*39*) to the scheme (*37*) does not improve the stability, in contrast with the formulation in velocities.

These instabilities have manifested themselves by strong oscillations on stress-time dependence far from the wall even if the implicite scheme of Crank–Nicolson type has been used. This defect has been suppressed by introducing an approximate analytical representation, the so-called creeping asymptote (*14*), of the stress field in the region far from the wall,

$$S(Y, T) \approx S(L, T) \cdot (H - Y)/(H - L) \quad \text{for} \quad Y \in (L, H), \tag{41}$$

with one unknown parametric function $S(L, T)$. It can be shown by an approach analogous to[3] that the creeping asymptote is a satisfactory approximation (relative errors of the instantaneous stresses less than 1%) for such a value of L which fulfils the inequality

$$0{\cdot}8 > \mathrm{Re}^*(L) \equiv (H - L)^2 \max |S(L, T)|^{m-1}. \tag{42}$$

The actual domain (Y, T) for solving the problem is diminished to an interior region at the wall, $0 < Y < L$, by using the analytical extrapolation (*41*) of stress profiles. The parametric function $S(L, T)$ should be determined by considering the new homogeneous boundary conditions of the 3rd kind,

$$(H - L)\,\partial_Y S\,|_{H=L} + S\,|_{Y=L} = 0\,. \tag{43}$$

Other group of difficulties arises at solving the problem in stresses due to the necessity to compute the stress gradients appearing in the both boundary conditions (*10*) and (*43*). The computation of the derivatives of a field on the boundary of the domain is notoriously known as a difficult problem suppressing considerably the attainable accuracy (errors about 20% of actual boundary values are typical). Diminishing the steps DY does not result in a satisfactory approach because of the necessity to hold $\beta < 1/2$ and, in effect, to diminish $DT \sim DY^2$. Such a thinning of the grid results in an unacceptable growth of the computational time, especially if the implicite schemes are used.

Decisive improvement of the approaches used until now was achieved by introducing discrete representations based on the integro-differential formulation of the equation of motion. The following integro-differential formulation

$$S(Y, T) = (H - Y)\,A(T) - \partial_T Q(Y, T)\,, \tag{44}$$

where

$$Q(Y, T) = \int_Y^H V(z, T)\,\mathrm{d}z =$$

$$= \int_0^Y (H - Y)\,[S(z, T)]^m\,\mathrm{d}z + \int_Y^H (H - z)\,[S(z, T)]^m\,\mathrm{d}z\,, \tag{45}$$

can be found by integrating Eq. (*1*) and using the all boundary conditions. The only supplementary constraint to the formulation (*44*) is the antiperiodicity condition.

The second integral on the r.h.s. of Eq. (*45*) can be expressed in the following way,

$$\int_Y^H (H - z)\,[S(z, T)]^m\,\mathrm{d}z =$$

$$= \int_Y^L (H - z)\,[S(z, T)]^m\,\mathrm{d}z + \frac{(H - L)^2}{m + 2}\,[S(L, T)]^m\,, \tag{46}$$

if the linear extrapolation (*41*) is introduced in the outer creeping region. In particular, the Eq. (*44*) is reduced to the form of the total macroscopic momentum balance,

$$S(0, T) = H\,A(T) - \partial_T Q(0, T)\,, \tag{47}$$

and of the macroscopic momentum balance for the outer creeping region,

$$S(L, T) = (H - L)\,A(T) - \partial_T Q(L, T)\,, \tag{48}$$

with the following simplified expressions of the total instantaneous flow rate,

$$Q(0, T) = \int_0^L (H - z)\,[S(z, T)]^m\,\mathrm{d}z + \frac{(H - L)^2}{m + 2}\,[S(L, T)]^m\,, \tag{49}$$

and the instantaneous flow rate in the outer region,

$$Q(L, T) = \int_0^L (H - L)\,[S(z, T)]^m\,\mathrm{d}z + \frac{(H - L)^2}{m + 2}\,[S(L, T)]^m\,. \tag{50}$$

The Eqs (*47*), (*48*) are used as substitutes for the undesirable boundary conditions (*10*), (*43*) of the 2nd and 3rd kind.

The corresponding finite-difference scheme is based on the common discrete representations of integro-differential operators in the sense of Crank and Nicolson[8], *i.e.* with the localization in the hypothetical central mesh point $(Y_j, T^{i+1/2})$ of a symmetrical cell with the six actual mesh points:

$$\partial_T [S]^m|_j^{i+1/2} = ([S_j^{i+1}]^m - [S_j^i]^m)/\mathrm{D}T\,, \tag{51}$$

$$\partial_{YY}^2 S|_j^{i+1/2} = (S_{j+1}^{i+1} - 2S_j^{i+1} + S_{j-1}^{i+1})/(2\,\mathrm{D}Y^2) + (S_{j+1}^i - 2S_j^i + S_{j-1}^i)/(2\,\mathrm{D}Y^2)\,, \tag{52}$$

etc.

The integrals Q in Eqs (*49*), (*50*) are represented in an analogous way, *i.e.* as the arithmetical averages of the integrals computed on the profiles T^i and T^{i+1}. The proper integration operator over an even number of intervals is represented by Simpson's quadrature formula:

$$\int_0^L (H - Y) f(Y)\,\mathrm{d}Y + \frac{(H - L)^2}{m + 2} f(L) = \mathrm{D}Y^2 \sum_{k=1}^{N} WJ_k f(Y_k)\,, \tag{53}$$

$$(H - L)\int_0^L f(Y)\,\mathrm{d}Y + \frac{(H - L)^2}{m + 2} f(L) = \mathrm{D}Y^2 \sum_{k=1}^{N} WW_k f(Y_k)\,, \tag{54}$$

where the coefficients WJ_k, WW_k are given by:

$$WJ_k = \begin{cases} w_k(HY + 1 - k)\,; & \text{for } k = 1, \ldots, N - 1 \\ w_k + \dfrac{HL^2}{m + 2}\,; & \text{for } k = N\,, \end{cases} \tag{55}$$

$$WW_k = \begin{cases} w_k HL; & \text{for} \quad k = 1, \ldots, N-1 \\ w_k HL + \dfrac{HL^2}{m+2}; & \text{for} \quad k = N. \end{cases} \tag{56}$$

The constants HY, HL depend on the dividing of the interval $Y \in (0; H)$ onto the inner (proper) and outer (linear) parts:

$$HY = (N-1)\,H/L, \quad HL = (N-1)\,(H-L)/L, \tag{57a, b}$$

the constants w_k are the common Simpson's coefficients:

$$w_k = \begin{cases} 1/3; & \text{for} \quad k = 1, \text{ or } k = N \\ 2/3; & \text{for} \quad k = 3, 5, \ldots, N-2 \\ 4/3; & \text{for} \quad k = 2, 4, \ldots, N-1. \end{cases} \tag{58}$$

This discrete representation results in the system of N non-linear algebraic equations. The common discrete representations of the differential formulation, Eq. (*9*), are included here for the inner mesh points, $j = 2, \ldots, N-1$:

$$[S_j^{i+1}]^m + \beta(2S_j^{i+1} - S_{j+1}^{i+1} - S_{j-1}^{i+1}) = [S_j^i]^m - \beta(2S_j^i - S_{j+1}^i - S_{j-1}^i). \tag{59}$$

In the boundary mesh points, $j = 1$ and $j = N$, the forementioned macroscopical balances of momentum in the discrete representation

$$\sum_{k=1}^{N} WJ_k[S_k^{i+1}]^m + \beta S_1^{i+1} = \sum_{k=1}^{N} WJ_k[S_k^i]^m - \beta S_1^i + 2\beta H\, A(T^{i+1/2}), \tag{60}$$

$$\sum_{k=1}^{N} WW_k[S_k^{i+1}]^m + \beta S_N^{i+1} = \sum_{k=1}^{N} WW_k[S_k^i]^m - \beta S_N^i + 2\beta(H-L)\, A(T^{i+1/2}), \tag{61}$$

are included.

In contrast to the tridiagonal Jacobian matrix typical for the Crank–Nicolson scheme, the considered finite difference scheme results in a system of equations with non zero off-diagonal elements in the Jacobian. An essential advantage of this scheme* consists in the identical fulfilling of the total momentum balance, $\varepsilon_M(T) = 0$.

It follows from the analytical estimate of the discretization errors that the integral formulas (*60*), (*61*) have errors of the order $0(DT^2 + DY^5)$, while the Crank–Nicolson scheme (*59*) includes errors of the order $0(DT^2 + DY^2)$. Thus, it appears mea-

* (it will be called BISS-scheme in the following text)

ningfull to increase the accuracy of finite-difference representations by accepting schemes which are based entirely on the integro-differential form (*44*) of the equations of motion.

The main problem which should be overcome in constructing the corresponding finite-difference scheme lies in adequate discrete representation of the integrals $Q(Y, T)$ in the points Y_j with the even indexes j. The following quadrature formulas have been chosen on the basis of numerical experiments with the integrand $f(z) = (a + z)^m$:

$$\int_{Y_j}^{Y_{j+1}} f(z)\,\mathrm{d}z = \frac{DY}{12}(5f_j + 8f_{j+1} - f_{j+2}) + \frac{(DY)^4}{24} f'''(\zeta)\,,$$

$$\int_{Y_{j+1}}^{Y_{j+2}} f(z)\,\mathrm{d}z = \frac{DY}{12}(-f_j + 8f_{j+1} + 5f_{j+2}) - \frac{(DY)^4}{24} f'''(\zeta)\,. \qquad (62a,b)$$

Here, $\zeta \in (Y_j;\ Y_{j+2})$ and f''' is a symbol for the 3rd derivative of the function f. The total of the both expressions in (*62a, b*) results in a well-known Simpson's formula:

$$\int_{Y_j}^{Y_{j+2}} f(z)\,\mathrm{d}z = \frac{DY}{3}(f_j + 4f_j + f_{j+2}) + \frac{(DY)^5}{90} f^{\mathrm{v}}(\zeta) \qquad (62c)$$

in which the discretization error is proportional to the 5th derivative of the function f. Even so, the suggested formulas (*62a, b*) are by an order more accurate than the trapezoidal formula with the error of the order $(DY)^3 f''(\zeta)/6$.

The quadrature formulas suggested result in the following discrete representation of the integration operator in Eq. (*45*):

$$\int_0^{Y_j} (H - Y_j) f(z)\,\mathrm{d}z + \int_{Y_j}^{L} (H - z) f(z)\,\mathrm{d}z = DY^2 \Big(\sum_{k=1}^{N} \lambda_{jk} f(Y_k)\Big)\,, \qquad (63)$$

where

$$\lambda_{jk} = \begin{cases} c_{jk} - 1/12\,; & \text{for even } j \text{ and } k = j + 1 \\ c_{jk}\,; & \text{for other } j,\ k\,, \end{cases} \qquad (64)$$

and

$$c_{jk} = \begin{cases} \left(\dfrac{N \,.\, H}{L} + 1 - j\right) w_k\,; & \text{for } \ 1 \leqq k \leqq j \\ \left(\dfrac{N \,.\, H}{L} + 1 - k\right) w_k\,; & \text{for } \ j \leqq k \leqq N\,. \end{cases} \qquad (65)$$

Numerical tests of the formula (54) for $f(z) = z^m$, $m \in (1; 10)$, $H = L = 2$, $N = 20$ have shown that the errors introduced by the discrete representation of the integral operator does not exceed 0·05% for $Y/L < 0{\cdot}8$ and 0·5% for $0{\cdot}8 < Y/L < 1$. Such an accuracy should be satisfactory for the majority of the finite-difference approximations.

The corresponding discrete representation of the considered boundary-value problem is constructed analogously with the BISS-scheme. The resulting system of the non-linear algebraic equations in the new SNOW-scheme has the following structure

$$\sum_{k=1}^{N} BB_{jk}[S_k^{i+1}]^m + \beta S_j^{i+1} = \sum_{k=1}^{N} BB_{jk}[S_k^i]^m - \beta S_j^i + 2\beta(H - Y_j)\, A(T^{i+1/2}), \quad (66)$$

where

$$BB_{jk} = \begin{cases} \lambda_{jk}\,; & \text{for} \quad k = 1, \ldots, N-1 \\ \lambda_{jk} + \dfrac{HL^2}{m+2}\,; & \text{for} \quad k = N\,. \end{cases} \quad (67)$$

The Jacobian of this system contains no zero elements. Therefore it should be expected that the treating of this system will be more time consuming than in the case of the BISS-scheme.

RESULTS AND DISCUSSIONS

The main reason for developing new finite-difference schemes based on the equation of motion in stresses lies in the uncertain accuracy of the results obtained by solving the problem in velocities. Our initial conjecture about the origin of considerable errors of the solution in velocities is documented in Fig. 2. The large defects of the macroscopical balances of momentum and energy have origin in the errors introduced by computing the velocity gradients at the wall, *i.e.* on the boundary of the domain.

The both new finite-difference schemes, BISS and SNOW, ensure the identical fulfilment of the instantaneous macroscopical balance of momemtun, $\varepsilon_M(T) = 0$, within accuracy of the order $0(DT^2 + DT^5)$. Thus, only the following error parameters remain to be tested:

(*i*) The accuracy of the iterative solution of the N non-linear equation system in every time step, which should fulfil the condition

$$\|(S_j^{i+1})_{k+1} - (S_j^{i+1})_k\| < \varepsilon_{it}\,. \quad (68)$$

(*ii*) The antiperiodicity of the solution characterized by the parameter ε_P.

(*iii*) The extent of the oscillations on the stress-time dependencies at $Y = \text{const.}$ (only qualitative test).

(*iv*) The accuracy of the total energy balance, which is characterized by the relative defect ε_E.

All the results discussed below have been obtained by realizing the schemes BISS and SNOW in the FORTRAN language on a computer EC 1033. The optimization procedure BSOLVE for solving the difficult systems of non-linear equation has been taken over from the literature[9]. All computations have been conducted in simple arithmetics.

The main problem in large-scale computations with a systematical series of the input parameters consisted in a considerable time consumption on the integration over the single period, $\Delta T = 2\pi$. Typical relevant data are presented in Table I.

The starting stress profiles (S_j^1) were either supplied as the input data or taken over from the previous integration. The acceptable periodicity condition, $\varepsilon_P(S) < 0{\cdot}005$, was obtained after integrating over $2 \div 3$ periods in the case of very good initial trials. The antiperiodicity condition, $\varepsilon_A(S) < 0{\cdot}005$, was however attained by far later, after $5 \div 10$ periods. Thus, the acceleration of the iterative process by the relaxation-type estimate of the new starting profile

$$(S_j^1)_{new} = \tfrac{1}{2}(S_j^{2M+1} - S_j^{M+1})_{old} \qquad (69)$$

can substantially reduce the total computational time.

The appearance of the local oscillations of stresses around the smoothed stress-time dependence presented some difficulties in testing the periodicity and antiperiodicity conditions. The effect of decreasing grid spacings on the extent of these local oscillations is demonstrated in Fig. 3 for rather unfavorable combination of parameters

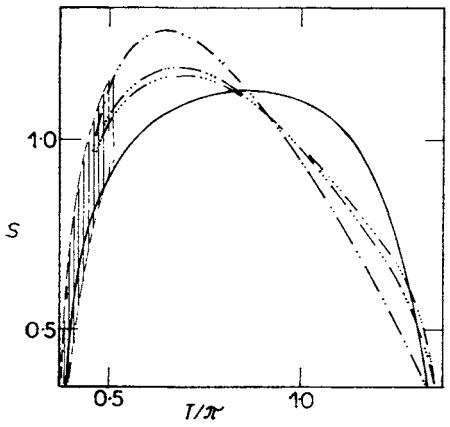

FIG. 2

Time course of stresses at the wall (data for $N = 20$, $M = 50$, $H = L = 10$, $n = 0{\cdot}15$, SNOW-scheme). Full line — actual course; dot-and-dashed lines — courses computed by numerical differentiation of the velocity profiles (the number of points on the line corresponds to the number of mesh points taken for the differentiation); hatched area — the region of strong local oscillations

TABLE I

Typical accuracies and time consumptions

Scheme	ε_{it}	N	M	ε_E	t (min)
BISS	10^{-2}	10	20	0·006	1
	10^{-2}	10	100	0·004	5
	10^{-2}	20	20	0·002	5
	10^{-3}	20	20	0·002	10
	10^{-3}	20	50	0·003	20
	10^{-3}	20	100	0·003	20
SNOW	10^{-3}	10	20	0·005	5
	10^{-3}	10	50	0·005	10
	10^{-3}	20	20	0·001	15
	10^{-3}	20	50	0·000	20
	10^{-4}	20	50	0·000	20
	10^{-4}	20	100	0·000	30

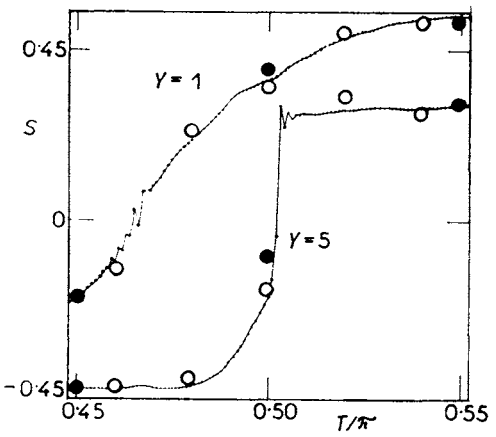

FIG. 3

Effect of the time step on the time course of stresses. Results of the computation using BISS-scheme for $n = 0{\cdot}15$, $H = L = 10$, $N = 20$. Time courses given for $Y = 1$ and $Y = 5$. Full points — $N = 20$, empty points — $N = 50$, dotted line — $N = 1\,000$. The computations executed for the common starting stress profil in the time $T_0 = 0{\cdot}4\,\pi$

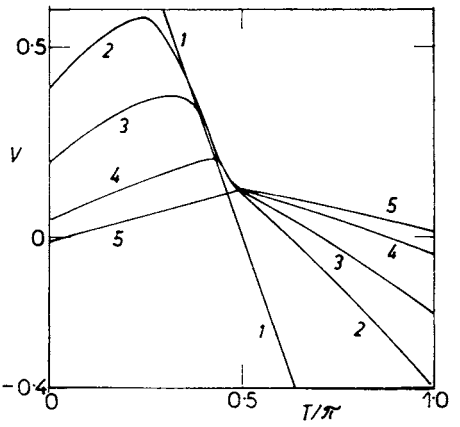

FIG. 4

Velocity field, the same run as in Fig. 2. Time courses of velocities are given for the following distances to the wall: 0 — 0·5 — 1·0 — 2·0 — 5·0 (curves *1* — *2* — *3* — *4* — *5*)

(m, H, L) and in the region of the most pronounced oscillation, *i.e.* in the region of rather stepwise change of stresses. It is apparent from Figs 3 and 5 that the values of stresses oscillate about the correct smoothed courses. Therefore, even the computations with relatively coarse grids result in acceptable accuracy of the macroscopic parameters[10]. In general, it can be concluded that the macroscopic parameters of the solution obtained for $N = 10$, $M = 50$, $\varepsilon_{it} = 0{\cdot}001$, $\varepsilon_P = 0{\cdot}005$ have not been changing more than about 0·5% of the actual values if thinner grids and more strict accuracy criteria have been supplied. The main effect of thinning the network consisted in smoothing the actual discrete representation of both the stress and velocity fields towards the courses predicted by the *ad hoc* smoothing procedure. Typical smoothed courses of the stresses and velocities show remarcable effect of the constitutive nonlinearity on the departure of these courses from the harmonic ones which are typical for the linear case, $m = 1$ (see Figs 4 and 5).

It was rather surprising finding that the velocity fields determined more than ten years ago[6] by the fast semiimplicite method are practically identical with the new results. In particular, the time courses of velocities depicted in Fig. 4 are identical for the all numerical methods used, within the limits of the graphical distinguishability.

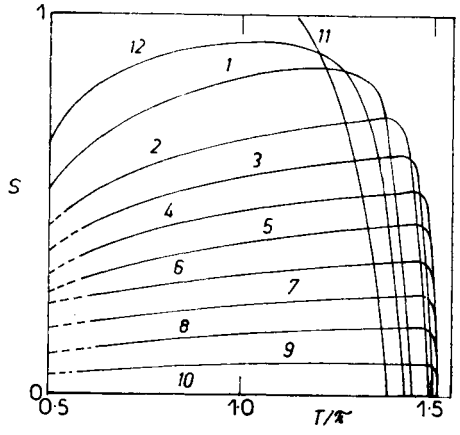

FIG. 5

Time courses of stresses, the same run as in Fig. 2. The label numbers *1—10* give the distances to the wall. The curves *11* and *12* correspond to $Y = 0$ and $Y = 0{\cdot}5$, resp. The hatched area distinguishes the region of local instabilities with low accuracy of results

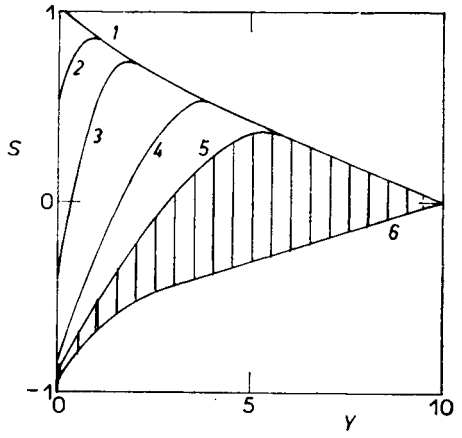

FIG. 6

Instantaneous stress profiles, the same run as in Fig. 2. Curves *1* — *2* — *3* — *4* — *5* — *6* correspond to the moments $T/\pi = 0{\cdot}9$ — 1·3 — 1·4 — 1·48 — 1·50 — 1·52; the hatched area corresponds to the interval $T/\pi \in (1{\cdot}50;$ 1·52) of the jump-like changes of stresses, compare with Fig. 5

It should be pointed out that the example considered here is one of the most difficult cases treated with the extreme non-linearity, $m = 6{\cdot}67$ and the boundary-layer regime, $H = 10$. The demonstrated coincidence can be taken as the definite confirmation of the correctness and accuracy of the gained numerical solutions.

The boundary-layer character of the oscillatory flow with a strong constitutive non-linearity is more apparent in terms of the stress field, as demonstrated in Figs 5 and 6. The instantaneous stress profiles near the wall immediately after changing the direction of flow are similar to ones for the start-up flow along the plate[11]. This picture of flow is radically changed in the moment when the stress signal reaches the free surface: the stress profiles become nearly linear and they are changing very slowly further on, compare Fig. 5.

The value $H = 10$ represents certain limit behind which the computations on a uniform grid with $DY = 0{\cdot}5$ would consume unacceptable computational time. Therefore, the computations for $H > 10$ have been carried out only by using the BISS-scheme with the linear extrapolation of the instantaneous stress profiles to the outer region, $5 = L < Y < H, N = 20, M = 50$. The resulting profiles of the instantaneous stress amplitudes

$$\bar{S}(Y) = \text{Max}\,|S(Y, T)|_{0<T<\pi} \tag{70}$$

are shown in Fig. 7. For the cases $H = 20$ and $H = 40$, it is apparent that the boundary-layer regime interferes with the outer region and so the condition (*42*) is not fulfiled. The cases treatable by the presented schemes are limited approximately by the condition $H \leqq 30$ if the additional constrains $DY \leqq 1$ (for saving the low discretization error) and $N \leqq 20$ (for saving the acceptable computational time) are taken into consideration.

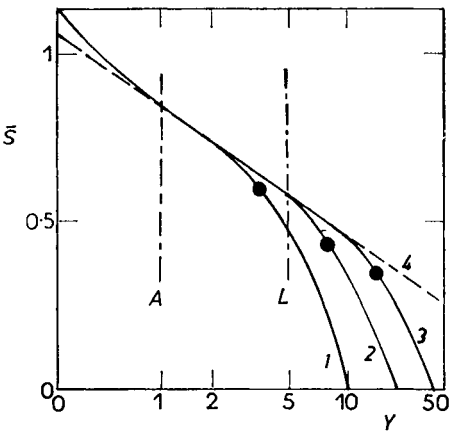

FIG. 7

Profiles of the stress amplitudes. Full lines *1*, *2*, *3* correspond to the cases $H = 10, 20, 40$ resp. at $n = 0{\cdot}15$. The dashed line *4* corresponds to the assumed similarity asymptote, $S \sim (1 + Y)^{-2/(m-1)}$. Full points on the curves characterize the actual boundary of the outer creeping region, $\text{Re}^*(Y) = 1$. *L* — boundary of the outer region as assumed in computations, *A* — probable boundary of the similarity boundary-layer region

It seems that this new limit in the numerical study of the non-Newtonian oscillatory boundary-layer flows can not be overcome by further improving finite-difference methods without introducing an adequate analytic asymptotic theory for $1 \ll Y \ll H$. It has been suggested quite recently[12] to develop such a theory assuming the existence of a transient similarity asymptote of the type

$$S(Y, T) \approx C(T - G(Y))\, F(Y)\,. \tag{71}$$

It can be easily found that only single class of the admissible solutions can exist, for which

$$G(Y) \sim (Y + Y_0)^{-1}\,, \quad F(Y) \sim (Y + Y_0)^{-2(m-1)}\,. \tag{72}$$

The good agreement of the numerical results with the assumption (*71*) is apparent from Fig. 7. if the choice $Y_0 = 1$ is made. This result is useful for the interpretation of the numerical results in the form of the estimate of the flow enhancement coefficient, given by Eqs (*19*), (*20*). It guarantees for $m > 1$ that the integral in the Eq. (*20*) is finite and, also, it provides an estimate of its asymptotical behaviour at $H \gg 1$:

$$\varkappa(m, H) \approx \varkappa(m, \infty) - \frac{\langle |C(T)|^{m-1} \rangle}{H + 1}\,. \tag{73}$$

The all known numerical data on the flow enhancement at higher H are presented in Fig. 8. The agreement between the asymptotical prediction by the formula (*68*) and the numerical data can be attained either by adjusting the value $\varkappa(m, \infty)$ empirically or by determining it as the arithmetical average of the two different analytical estimates[3,4]. The deviations from the asymptotical behaviour predicted by the for-

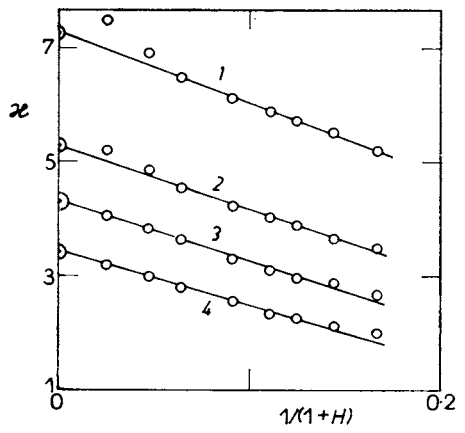

FIG. 8

Resulting estimates of the flow enhancement under boundary-layer regime. The inner points represent the numerical results determined by using BISS-scheme, the side points represent the approximate analytical result. Straight lines are fitted empirically. *m*: *1* 6·7, *2* 4·0, *3* 3·0, *4* 2·0

mula (*68*) can be attributed to the interference of the boundary-layer and creeping zones of flow, *i.e.* to the improper choice of the interface boundary, $Y = L$, for the linear extrapolation of the stress profiles.

CONCLUSION

The earlier numerical solutions to the problem of non-Newtonian oscillatory flows based on the formulation in velocities did not gave a chance to a quantitative testing of accuracy of the results. The presented novel finite-difference methods based on the integro-differential formulation in stresses give the results of the excellent and guarranted accuracy but they are rather cumbersome in view of the necessary computational time. The comparison of the old and new results has shown that the earlier numerical solutions gave also accurate data on the most important macroscopic parameters, *e.g.* the flow enhancement.

The resulting numerical estimates of the flow enhancement at the high but finite values of the modified Reynolds number, $H = 10$, are compatible with the former analytical estimates at $H = \infty$.

LIST OF SYMBOLS

$a\omega^2 = \max \lvert\dot{u}(t)\rvert$	maximum acceleration of the oscillating plate
$A = -\dot{u}/(a\omega^2)$	normalized acceleration of the oscillating plate
$DT = 2\pi/(2M + 1)$	step on the time coordinate
$DY = L/(N - 1)$	step on the space coordinate
E	coefficient of flow enhancement, see Eq. (*19*)
Fr $a\omega^2/g_z$	Froude number for oscillatory flow
g_z	longitudinal component of gravity acceleration
h	thickness of the liquid film on the oscillating plate
H h/δ_B	modified Reynolds number for oscillatory flows
HY, HL	parameters of the quadrature formulas (*53*), (*54*)
i	sequential index on the time coordinate
j	sequential index on the space coordinate
k	summation index on the space coordinate
L	boundary of the grid region
m $1/n$	reciprocal flow index
n	flow index, the parameter of the power-law viscosity function, $\tau_{zy} = K[-\partial_y v_z]^n$
M	number of the mesh points on the time coordinate for the half-period
N	number of the mesh points on the space coordinate
Q	normalized instantaneous volumetric flow rate, see Eq. (*45*)
Re*	local Reynolds number, see Eq. (*42*)
$S = \tau_{yz}/\sigma_B$	normalized stress
S_j^i	values of $S(Y, T)$ in the mesh points
t	time
$T = \omega t$	normalized time
T^i	mesh point value of T

$u(t)$	instantaneous velocity of the oscillating plate
v_z	velocity of liquid
$V = v_z/(a\omega)$	normalized velocity of liquid
V_j^i	values of $V(Y, T)$ in the mesh points
$V_0 = u/(a\omega)$	normalized velocity of the oscillating plate
w_k	Simpson's coefficients, Eq. (*58*)
y	distance from the plate
$Y = y/\delta_B$	normalized distance from the plate
Y_j	mesh point value of Y
$\alpha = DT/DY^{1+n}$	inertia parameter for the finite-difference schemes in velocities
$\beta = \frac{1}{2} DT/DY^2$	inertia parameter for the finite-difference schemes in stresses
$\delta_B = (K^m \varrho^{-m} a^{-m+1} \omega^{-2m+1})^{1/(1+m)}$	characteristic thickness of the oscillatory boundary-layer
ε_{it}	error parameter, Eq. (*68*)
ε_P	boundary deviation from the periodicity condition, Eq. (*24a*)
ε_A^*	domain deviation from the antiperiodicity condition, Eq. (*24c*)
ε_A	boundary deviation from the antiperiodicity condition, Eq. (*24b*)
ε_M	defect of the macroscopic momentum blaance, Eq. (*25*)
ε_E	defect of the total energy balance, Eq. (*26*)
$\varkappa(m, H)$	function defined by Eq. (*20*)
τ_{yz}	instantaneous local shear stress
$\tau_B = (K^m \varrho a^2 \omega^3)^{1/(1+m)}$	characteristic amplitude of the oscillatory stresses under the boundary-layer condition
Ψ_{work}, Ψ_{diss}	normalized total work of the oscillatory plate, normalized viscous dissipation
$\omega = 2\pi/\theta$,	angular frequency of the process with the period θ
$\|B_j\| = \max \|B_j\|$	vector norm
$\|B_j^i\| = \max \|B_j^i\|$	matrix norm
$\langle f(T) \rangle = \frac{1}{2\pi} \int_0^{2\pi} f(T)\, dT$	time mean of the periodic function $f(T)$
$[x]^p = \text{sign}\,(x)\,\|x\|^p$	odd power-law function

REFERENCES

1. Sobolík V., Wein O., Mitschka P.: Rheol. Acta *16*, 394 (1977).
2. Wein O., Sobolík V.: This Journal *45*, 1010 (1980).
3. Wein O.: This Journal *48*, 1579 (1983).
4. Wein O., Sobolík V.: Chem. Prům. *28*, 161 (1978).
5. Wein O.: This Journal *44*, 2908 (1979).
6. Sobolík V., Mitschka P.: *Numerical Solution of Parabolic Equations with an Essential Nonlinearity*. Proc. 5th Symp. "*Computers in Chemical Engineering*", Czechoslovakia, Vysoké Tatry 1977 (Ed. M. Kubíček).
7. Wein O.: *Numerické řešení úlohy o oscilační mezní vrstvě v nenewtonských kapalinách*. Report 15/1984, ÚTZCHT, ČSAV, Praha 1984.
8. Kubíček M.: *Numerické algoritmy řešení chemicko-inženýrských úloh*. SNTL, Praha 1983.
9. Kuester J. L., Mize J. H.: *Optimization Techniques with* FORTRAN. McGraw-Hill, 1973.
10. Wein O., Mitschka P.: Rheol. Acta *17*, 463 (1978).
11. Bird R. B.: AIChE J. *5*, 565 (1959).
12. Wein O., Mitschka P.: J. Non-Newt. Fluid Mech., in press.

Translated by the author (O. W.).